Journal of Organometallic Chemistry 706-707 (2012) 20–25

Contents lists available at SciVerse ScienceDirect

Journal of Organometallic Chemistry

journal homepage: www.elsevier.com/locate/jorganchem

Iridium–Ruthenium–gold cluster complexes: Structures, and skeletal Rearrangements

Richard D. Adams*, Perry J. Pellechia, Mark D. Smith, Qiang Zhang

Department of Chemistry and Biochemistry, University of South Carolina, Columbia, SC 29208, USA

ARTICLE INFO

Article history:
Received 11 November 2011
Received in revised form
23 December 2011
Accepted 9 January 2012

Keywords:
Cluster
Trimetallic
Gold
Iridium
Ruthenium

ABSTRACT

Three new IrRuAu trimetallic cluster complexes: $IrRu_3(CO)_{13}AuPPh_3$, **1**, $HIrRu_3(CO)_{12}(AuPPh_3)_2$, **2** and $IrRu_3(CO)_{12}(AuPPh_3)_3$, **3** were obtained in low yields from the reaction of $HIrRu_3(CO)_{13}$ with $[(AuPPh_3)_3O][BF_4]$. Compounds **1** and **3** were subsequently obtained in much better yields (82%) and (84%) from the reactions of $[AuPPh_3][NO_3]$ and $[(AuPPh_3)_3O][BF_4]$ with $[PPN][IrRu_3(CO)_{13}]$, respectively. The molecular structures of all three compounds were established by single crystal x-ray diffraction methods. Compounds **1** and **2** contain an $Au(PPh_3)$ group that bridges one triangular face of a tetrahedral $IrRu_3$ cluster. Compound **2** contains a second $Au(PPh_3)$ capping group that bridges an Ir–Ru–Au triangle. Compound **3** consists of a pentagonal bipyramidal Au_3IrRu_3 cluster that has three gold atoms and two of the ruthenium atoms in the equatorial plane. There is a bond between the apical Ir and Ru atoms. Compounds **2** and **3** exhibit dynamical activity in the metal skeleton that leads to a rapid averaging of the inequivalent $Au(PPh_3)$ groups on the NMR timescale at room temperature.

1. Introduction

Applications for iridium in catalysis continue to grow [1]. Although most catalytic applications are of a homogeneous type [1,2], it has been shown that iridium complexes can also serve as precursors to catalysts that exhibit good activity for the hydrogenation of aromatics and olefins when placed on supports [3]. Heterogeneous iridium-iron catalysts derived from bimetallic cluster complexes have been shown to exhibit good catalytic activity for the formation of methanol from synthesis gas. [4]. Iridium–ruthenium complexes have been shown to serve as precursors to catalysts for the carbonylation methanol [5]. Supported bimetallic iridium–ruthenium catalysts have been shown to produce C_2 oxygenates from syngas [6] and also to exhibit unusually high catalytic activity for the oxygen evolution reaction in the electrolysis of water [7]. Recently, gold nanoparticles have been shown to exhibit significant catalytic activity for the oxidation of CO and certain olefins [8]. Combining transition metals with gold has led to interesting new bimetallic oxidation nanocatalysts [9].

There have been very few structural characterizations of iridium–ruthenium–gold carbonyl cluster complexes [10]. In the course of our studies of the chemistry of $[IrRu_3(CO)_{13}]^-$ [11], we have investigated its reactions with $[AuPPh_3]NO_3$ and $[(AuPPh_3)_3O][BF_4]$. We have obtained three new iridium–ruthenium–gold carbonyl cluster complexes, have established their molecular structures and have investigated their properties in solution. These results are reported herein.

2. Experimental

General Data. Reagent grade solvents were dried by the standard procedures and were freshly distilled prior to use. Infrared spectra were recorded on a Thermo Nicolet Avatar 360 FT-IR spectrophotometer. Room temperature ^1H NMR and $^{31}P\{^1H\}$ NMR were recorded on a Bruker Avance/DRX 400 NMR spectrometer operating at 400.3 and 162.0 MHz, respectively. Different temperature $^{31}P\{^1H\}$ NMR for compound **3** were recorded on a Varian Mercury 400 spectrometer operating at 161.9 MHz ^{31}P $\{^1H\}$ NMR spectra were externally referenced against 85% *o*-H_3PO_4. Positive/negative ion mass spectra were recorded on a Micromass Q-TOF instrument by using electrospray (ES) ionization. $Ru_3(CO)_{12}$ and $Ir_4(CO)_{12}$ were obtained from STREM and were used without further purification. $HIrRu_3(CO)_{13}$ [12], $[PPN][IrRu_3(CO)_{13}]$ [12], $[AuPPh_3][NO_3]$ [13] and $[(AuPPh_3)_3O][BF_4]$ [14] were prepared according to the previously reported procedures. Product separations were performed by TLC in air on Analtech 0.25 silica gel 60 Å F254 glass plates. Dynamic NMR simulations for compound **3** were performed by using the SpinWorks program [15]. The exchange rates were determined at seven different temperatures in the temperature range −60 to +20 °C. The activation parameters were determined from a least-

* Corresponding author.
E-mail address: Adams@mail.chem.sc.edu (R.D. Adams).

0022-328X/$ – see front matter © 2012 Elsevier B.V. All rights reserved.
doi:10.1016/j.jorganchem.2012.01.012

squares Eyring plot by using the program Microsoft Excel 2007: $\triangle H^{\ddagger} = 48.8(5)$ kJ mol^{-1}, $\triangle S^{\ddagger} = 17.3(5)$ J mol^{-1} K^{-1}.

2.1. Reaction of $HIrRu_3(CO)_{13}$ with $[(AuPPh_3)_3O][BF_4]$

A mixture of 18.70 mg (0.01263 mmol) of $[(AuPPh_3)_3O][BF_4]$ and 21.35 mg (0.02481 mmol) of $HIrRu_3(CO)_{13}$ was stirred in 30 mL of THF for 2 h. The solvent was removed in vacuo, and the product was then isolated by TLC by using a 4:1 hexane/methylene chloride solvent mixture to yield in order of elution the following: 5.8 mg (36.8%) of $Ru_3(CO)_{12}$, 1.2 mg (6.3%) of $H_2Ru_4(CO)_{13}$, 2.3 mg (7% yield) of $IrRu_3(CO)_{13}AuPPh_3$, **1**, 3.2 mg (7.3% yield) of $HIrRu_3(CO)_{12}(AuPPh_3)_2$, **2** and 1.6 mg (2.9% yield) of $IrRu_3(CO)_{12}(AuPPh_3)_3$, **3**, and some uncharacterized compounds. Spectral data for **1**: IR ν_{CO} (cm^{-1} in CH_2Cl_2): 2084(m), 2041(s), 2007(m), 1990(m), 1844(*w*). ^{1}H NMR (CD_2Cl_2, 25 °C, TMS) δ = 7.29–7.55 (m, 15H, Ph). ^{31}P{^{1}H} NMR (CD_2Cl_2, 25 °C), δ = 73.85 (s,1P, P–Au). Mass Spec: ES-/MS m/z = 1365 (M + CO_2H^-). Spectral data for **2**: IR ν_{CO} (cm^{-1} in CH_2Cl_2): 2070(s), 2046(s), 2009(vs), 1961(m), 1809(*w*). ^{1}H NMR (CD_2Cl_2, 25 °C, TMS) δ = 7.08–7.52 (m, 30H, Ph), δ = −17.43 (s, 1H, hydride). ^{31}P{^{1}H} NMR (CD_2Cl_2, 25 °C) δ = 70.20 (s, 2P); at −80 °C in CD_2Cl_2: δ = 70.23 (s, 1P), 67.67 (s, 1P). Mass Spec: ES+/MS, m/z = 1752 M$^+$. Spectral data for **3**: IR ν_{CO} (cm^{-1} in CH_2Cl_2): 2051(vs), 2010(vs), 1986(s), 1955(m), 1914(*w*), 1784(br). ^{1}H NMR (CD_2Cl_2, 25 °C, TMS) δ = 7.12–7.33 (m, 45H, Ph). ^{31}P{^{1}H} NMR (CD_2Cl_2, 25 °C) δ = 65.59 (s, 3P, P–Au); at −80 °C δ = 68.47 (2P) and 58.00 (1P). Mass Spec: ES+/MS, m/z = 2210.

2.2. Improved synthesis of $IrRu_3(CO)_{13}AuPPh_3$, **1**

11.2 mg (0.0215 mmol) of $[AuPPh_3][NO_3]$ was added to a 100 mL three neck flask with a solution of 30.0 mg (0.0215 mmol) [PPN] $[IrRu_3(CO)_{13}]$ in 30 mL THF. The solvent was removed in vacuo after 15 min at room temperature, and the product was then isolated by TLC using a 4:1 hexane/methylene chloride solvent mixture: 23.3 mg of **1** (82% yield) was obtained.

2.3. Improved synthesis of **3**

To a 100 mL three neck flask, 25.8 mg (0.0174 mmol) of $[(AuPPh_3)_3O][BF_4]$ was added to 24.37 mg (0.0174 mmol) of [PPN] $[IrRu_3(CO)_{13}]$ dissolved in 30 mL of THF. After 2h at 25 °C, the solvent was removed in vacuo, and the product was then isolated by TLC using a 2:1 hexane/methylene chloride solvent mixture. 32.24 mg of **3** (84% yield) was obtained.

2.3.1. Crystallographic analyses

Red single crystals of **1**, orange single crystals of **2** and black single crystals of **3** suitable for x-ray diffraction analyses were all obtained by slow evaporation of solvent from solutions of the pure compounds in hexane/methylene chloride solvent mixture at −25 °C. Each data crystal was glued onto the end of a thin glass fiber. X-ray intensity data were measured by using a Bruker SMART APEX CCD-based diffractometer by using Mo Kα radiation (λ = 0.71073 Å). The raw data frames were integrated with the SAINT + program by using a narrow-frame integration algorithm [16]. Correction for Lorentz and polarization effects were also applied using SAINT+. An empirical absorption correction based on the multiple measurement of equivalent reflections was applied using the program SADABS. All structures were solved by a combination of direct methods and difference Fourier syntheses, and were refined by full-matrix least-squares on F^2 by using the SHELXTL software package [17]. All non-hydrogen atoms were refined with anisotropic displacement parameters. Hydrogen atoms were placed in geometrically idealized positions and included as standard riding atoms during the least-squares refinements. Crystal data, data collection parameters, and results of the analyses are listed in Table 1.

Compound **1** crystallized in the monoclinic crystal system. The space group $P2_1/n$ was indicated by the unique pattern of systematic absences observed in the data and was confirmed by the successful solution and refinement of the structure. Compounds **2** and **3** both crystallized in the triclinic crystal system. The space group $P\bar{1}$ was assumed in both cases and was confirmed by the successful solutions and refinements of the structures. For the structure of **2**, there were two independent molecules of the complex and two hexane molecules from the crystallization solvent present in the asymmetric unit. The hydride ligand was located along one of the Ru–Ru bonds in each molecule. The hydride ligand in both molecules was refined with fixed Ru–H bond distances (1.75Å). The iridium atom Ir(1) and the ruthenium atom Ru(3) in

Table 1
Crystallographic data for compounds **1**–**3**.

Compound	**1**	**2**	**3**
Empirical formula	$C_{31}H_{15}O_{13}PAuIrRu_3$	$C_{48}H_{31}O_{12}P_2Au_2IrRu_3 \cdot C_6H_{14}$	$C_{66}H_{45}O_{12}P_3Au_3IrRu_3$
Formula weight	1318.78	1837.18	2209.24
Crystal system	Monoclinic	Triclinic	Triclinic
Lattice parameters			
a (Å)	16.6814(6)	13.7813(6)	13.4662(3)
b (Å)	9.7331(4)	20.8227(9)	14.7194(3)
c (Å)	22.0846(8)	20.8318(9)	19.1092(4)
α (deg)	90	90.055(1)	107.322(1)
β (deg)	99.996(1)	100.701(1)	99.010(1)
γ (deg)	90	96.540(1)	109.378(1)
V (Å^3)	3531.3(2)	5834.3(4)	3271.04(12)
Space group	$P2_1/n$	$P-1$	$P-1$
Z value	4	4	2
ρcalc (g/cm^3)	2.481	2.092	2.243
μ (Mo Kα) (mm-1)	9.257	8.150	9.534
Temperature (K)	294(2)	294(2)	293(2)
2Θ max (°)	50.04	48.22	50.04
No. Obs. ($I > 2\sigma(I)$)	6239	18532	11556
No. Parameters	451	1161	794
Goodness of fit (GOF)	1.096	1.026	1.094
Max. shift in cycle	0.001	0.002	0.001
Residuals[a]: R1; wR2	0.0220; 0.0545	0.0686; 0.1413	0.0321; 0.0734
Absorption Correction Max/min	1.000/0.423	1.000/0.689	1.000/0.628
Largest peak in Final Diff. Map (e$^-$/Å^3)	2.146	1.738	4.287

[a] $R = \Sigma_{hkl}(||F_{obs}|-|F_{calc}||)/\Sigma_{hkl}|F_{obs}|$; $R_w = [\sum_{hkl} w(|F_{obs}| - |F_{calc}|)^2/\sum_{hkl} wF_{obs}^2]^{1/2}$; $w = 1/\sigma^2(F_{obs})$; GOF = $[\Sigma_{hkl} w(|F_{obs}|-|F_{calc}|)^2/(n_{data}-n_{vari})]^{1/2}$.

compound **3** were disordered in the solid state. The occupancies of these two atoms were refined by using EXYZ and EADP constraints. The occupancies in the final cycle of refinement were 0.78/0.22.

3. Results and discussion

Three new IrRuAu compounds: $IrRu_3(CO)_{13}(AuPPh_3)$, **1** (7% yield), $HIrRu_3(CO)_{12}(AuPPh_3)_2$, **2** (7.3% yield) and $IrRu_3(CO)_{12}(AuPPh_3)_3$, **3** (2.9% yield) were obtained from the reaction of $HIrRu_3(CO)_{13}$ with $[(AuPPh_3)_3O][BF_4]$. Compounds **1** and **3** were subsequently obtained in much better yields (82%) and (84%) from the reactions of $[AuPPh_3][NO_3]$ and $[(AuPPh_3)_3O][BF_4]$ with [PPN] $[IrRu_3(CO)_{13}]$, respectively, see Scheme 1. Each of the new complexes was characterized by a combination of IR, ^1H NMR, mass spectral and single crystal X-ray diffraction analyses.

An ORTEP diagram of the molecular structure of compound **1** is shown in Fig. 1. The basic framework of the $IrRu_3Au$ metal cluster in **1** is best described as an Au-capped $IrRu_3$ tetrahedron. The Au atom caps the Ru_3 triangle. The Ru–Au distances in **1** span a considerable range, Au(1)–Ru(1) = 3.0056(4) Å, Au(1)–Ru(2) = 2.8063(4) Å, Au(1)–Ru(3) = 2.7486(4) Å, and this may be related to the unsymmetric distribution of the CO ligands on the Ru atoms, see below. Compound **1** is similar to the $CoRu_3Au$ compound $CoRu_3(CO)_{13}AuPPh_3$, **4**, but in **4** the Au atom caps one of the $CoRu_2$ triangles of the $CoRu_3$ tetrahedron [18]. For comparison, the Au–Ru distances in **4** are 2.776(1) Å and 2.774(1) Å. Two of the three Ru–Ru bonds in **1** contain bridging CO ligands and the associated Ru–Ru bond distances, Ru(1)–Ru(2) = 2.8266(5) Å, Ru(1)–Ru(3) = 2.7918(5) Å, are significantly shorter than the third Ru–Ru bond distance, Ru(2)–Ru(3) = 3.0064(5) Å, which has no bridging CO ligand. The Ir–Ru bond distances, Ir(1)–Ru(1) = 2.7586(4) Å, Ir(1)–Ru(2) = 2.7336(4) Å, and Ir(1)–Ru(3) = 2.7643(4) Å, are similar to the Ir–Ru bond distances, 2.680(4) Å–2.771(5) Å in the compound $[PPh_4][Ir_6Ru_3(CO)_{21}(AuPPh_3)]$[10a] which contains $Ru(CO)_3$ capping groups on three triangular faces of an Ir_6 octahedron. If the $AuPPh_3$ group is considered as a one electron donor to the $IrRu_3$ tetrahedron, then the $IrRu_3$ cluster contains a total of 60 valence electrons which means that the Ir atom and each of the Ru atoms formally have 18 electron configurations.

An ORTEP diagram of the molecular structure of compound **2** is shown in Fig. 2. The metal cluster in **2** can be described as an $Au(PPh_3)$ capped trigonal-bipyramidal $AuIrRu_3$ cluster, but this $AuIrRu_3$ cluster is not the same as that in **1**. The Au atom in $AuIrRu_3$ cluster in **2** caps an $IrRu_2$ triangle not the Ru_3 triangle as in **1** and the $Au(PPh_3)$ cap on that bridges one of the AuIrRu triangles. The Au–Au bond distance, Au(1)–Au(2) = 2.8563(10) Å, is slightly longer than the Au–Au bond distance in the Au_2CoRu_3 compound $HCoRu_3(CO)_{13}(AuPPh_3)_2$, **5**, 2.787 (1) Å, which contains an $Au(PPh_3)$ capping group on a trigonal-bipyramidal $AuCoRu_3$ cluster that has a similar structure to **2**.[10a] Compound **2** contains one hydride ligand, $\delta = -17.43$ in the H NMR spectrum, which was found to bridge the Ru(1)–Ru(2) bond. As a result, the associated Ru(1)–Ru(2) bond distance is elongated, 2.992(2) Å, due to the presence of this ligand [19]. Otherwise, the Ir–Ru and Ru–Ru distances in **2** are similar to those observed in **1**. Compound **2** exhibits only one phosphorus resonance at $\delta = 70.20$ in its ^{31}P NMR spectrum at room temperature, but it shows two resonances as expected at $\delta = 70.23$ and 67.67 at −80 °C. This temperature dependence can be explained by a dynamical exchange process that leads to an interchange of the environments of the two inequivalent $Au(PPh_3)$ groups in **2** on the NMR timescale at room temperature. A possible mechanism is illustrated by shifts of the Au_2 group to each of the $IrRu_2$ triangles by using the Ir atom as a pivot point such as shown in Scheme 2.

A number of examples of similarly structured metal cluster complexes containing $Au(PPh_3)$ groups have been reported to exhibit similar molecular dynamics [20]. As in **1**, if each of the $AuPPh_3$ group is considered as a one electron donor to the $IrRu_3$ tetrahedron, then the $IrRu_3$ cluster contains a total of 60 valence

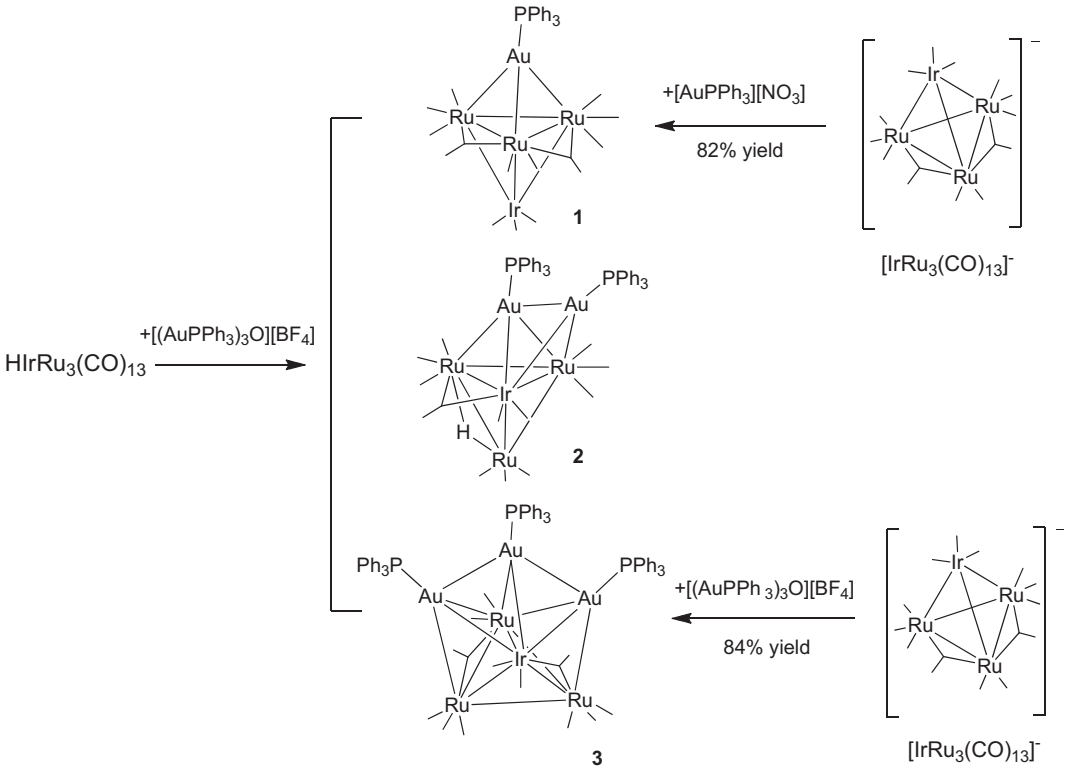

Scheme 1. $IrRu_3Au_n$ complexes obtained from reaction of $IrRu_3$ complexes with Au cations.

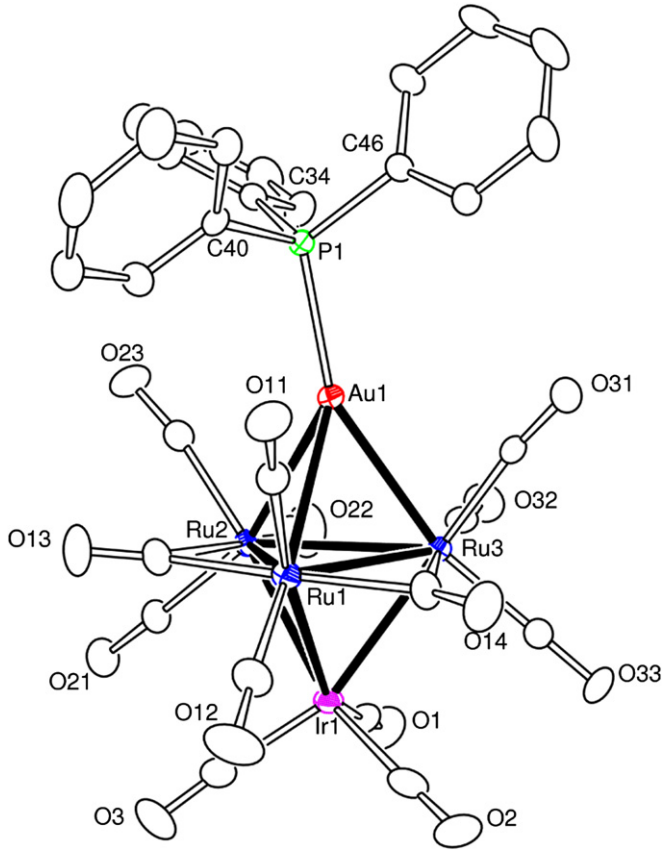

Fig. 1. An ORTEP diagram of the molecular structure of $IrRu_3(CO)_{13}(AuPPh_3)$, 1 showing 20% thermal ellipsoid probabilities. Selected interatomic bond distances (Å) and angles (o) are as follows: Au(1)–Ru(1) = 3.0056(4), Au(1)–Ru(2) = 2.8063(4), Au(1)–Ru(3) = 2.7486(4), Ir(1)–Ru(1) = 2.7586(4), Ir(1)–Ru(2) = 2.7336(4), Ir(1)–Ru(3) = 2.7643(4), Ru(1)–Ru(2) = 2.8266(5), Ru(1)–Ru(3) = 2.7918(5), Ru(2)–Ru(3) = 3.0064(5); Au(1)–Ru(1)–Ir(1) = 102.433(12), Au(1)–Ru(2)–Ir(1) = 108.489(13), Au(1)–Ru(2)–Ir(1) = 109.278(13).

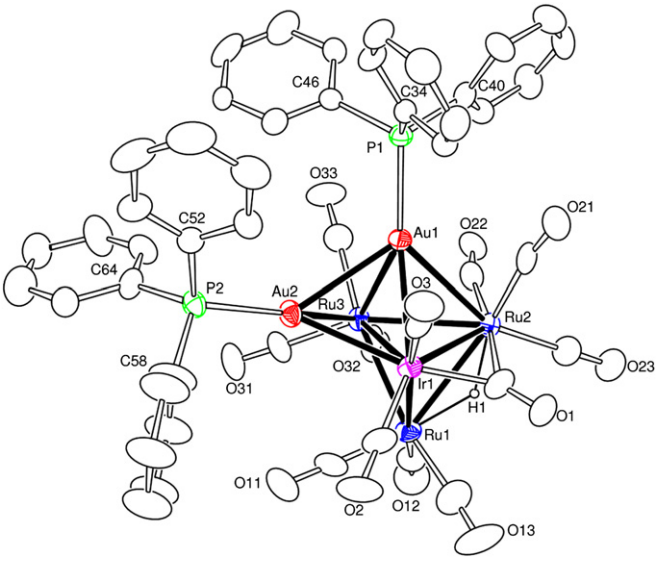

Fig. 2. An ORTEP diagram of the molecular structure of $HIrRu_3(CO)_{12}(AuPPh_3)_2$, 2 showing 20% thermal ellipsoid probabilities. Selected interatomic bond distances (Å) and angles (o) are as follows: Au(1)–Au(2) = 2.8563(10), Au(1)–Ir(1) = 2.7769(10), Au(1)–Ru(2) = 3.0746(16), Au(1)–Ru(3) = 2.8049(15), Au(2)–Ir(1) = 2.7908(10), Au(2)–Ru(3) = 2.8555(16), Ir(1)–Ru(1) = 2.7597(17), Ir(1)–Ru(2) = 2.7915(16), Ir(1)–Ru(3) = 2.9606(16), Ru(1)–Ru(2) = 2.992(2), Ru(1)–Ru(3) = 2.749(2), Ru(2)–Ru(3) = 2.9621(19); Au(1)–Ir(1)–Ru(1) = 111.91(4), Au(1)–Ru(2)–Ru(1) = 98.25(5), Au(1)–Ru(3)–Ru(1) = 111.38(6), Au(1)–Au(2)–Ru(3) = 58.82(3), Au(1)–Au(2)–Ir(1) = 58.90(3), Au(2)–Au(1)–Ru(2) = 105.67(4), Au(2)–Ir(1)–Ru(1) = 101.18(4), Au(2)–Ir(1)–Ru(2) = 115.77(4), Au(2)–Ru(3)–Ru(1) = 99.84(6), Au(2)–Ru(3)–Ru(2) = 108.72(5).

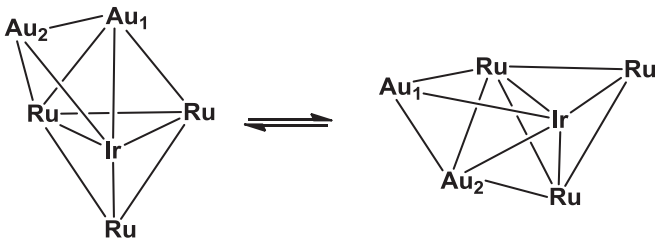

Scheme 2. A proposed mechanism for the dynamical averaging of the $Au(PPh_3)$ groups in compound **2**.

electrons and the Ir atom and each of the Ru atoms formally have 18 electron configurations.

An ORTEP diagram of the molecular structure of compound **3** is shown in Fig. 3. Compound **3** contains three $Au(PPh_3)$ groups combined with the $IrRu_3$ cluster of the original reagents $HIrRu_3(CO)_{13}$ or anion $[IrRu_3(CO)_{13}]^-$. The metal cluster in **3** can be described in different ways. It could be described as an $IrRu_3$ tetrahedron with three bridging three $Au(PPh_3)$ groups. Alternatively, the cluster could be described as a seven atom pentagonal bipyramidal Au_3IrRu_3 cluster with an additional bond between the apical atoms Ir(1) and Ru(3), Ir(1) - Ru(3), 2.8770(5) Å. The other Ir–Ru bond distances are Ir(1)–Ru(1) = 2.8406(6) Å and Ir(1)–Ru(2) = 2.9387(6) Å. There are two bridging CO ligands that bridge the Ir(1)–Ru(1) and Ru(2)–Ru(3) bonds. The $Au(PPh_3)$ groups are mutually bonded, but the Au–Au bond distances, Au(1)–Au(2) = 2.9781(4) Å, Au(1)–Au(3) = 2.9726(4) Å, are significantly longer than that in **2**, but are still within the normal bonding range. For comparison, the Au–Au bond distances in the octahedral hexagold complex$[Au_6\{P\text{-}p\text{-}tolyl_3\}][BPh_4]_2$ range from 2.932(2) Å–3.091(2) Å [21]. If one considers compound **3** as a $IrRu_3$

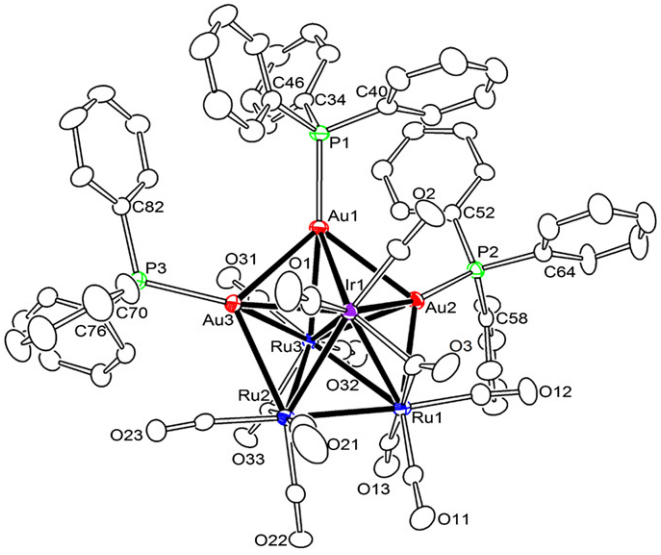

Fig. 3. An ORTEP diagram of the molecular structure of $IrRu_3(CO)_{12}(AuPPh_3)_3$, 3 showing 20% thermal ellipsoid probabilities. Selected interatomic bond distances (Å) and angles (o) are as follows: Au(1)–Au(2) = 2.9781(4), Au(1)–Au(3) = 2.9726(4), Au(1)–Ir(1) = 2.8243(4), Au(1)–Ru(3) = 2.8692(5), Au(2)–Ir(1) = 2.8829(4), Au(2)–Ru(1) = 2.8878(6), Au(2)–Ru(3) = 2.7596(5), Au(3)–Ir(1) = 2.8107(4), Au(3)–Ru(2) = 2.9674(6), Au(3)–Ru(3) = 2.8206(5), Ir(1)–Ru(1) = 2.8406(6), Ir(1)–Ru(2) = 2.9387(6), Ir(1)–Ru(3) = 2.8770(5), Ru(1)–Ru(2) = 2.8334(8), Ru(1)–Ru(3) = 3.0959(7), Ru(2)–Ru(3) = 2.8895(7); Au(1)–Ir(1)–Ru(1) = 116.201(16), Au(1)–Ir(1)–Ru(2) = 112.975(16), Au(1)–Au(2)–Ru(1) = 110.138(14), Au(1)–Au(3)–Ru(2) = 107.993(14), Au(2)–Au(1)–Au(3) = 103.828(10), Ir(1)–Au(1)–Ru(3) = 60.698(11), Au(2)–Ir(1)–Au(3) = 110.692(13), Au(2)–Ru(3)–Au(3) = 114.137(16), Au(2)–Ru(1)–Ru(2) = 107.14(2), Au(3)–Ru(2)–Ru(1) = 108.75(2).

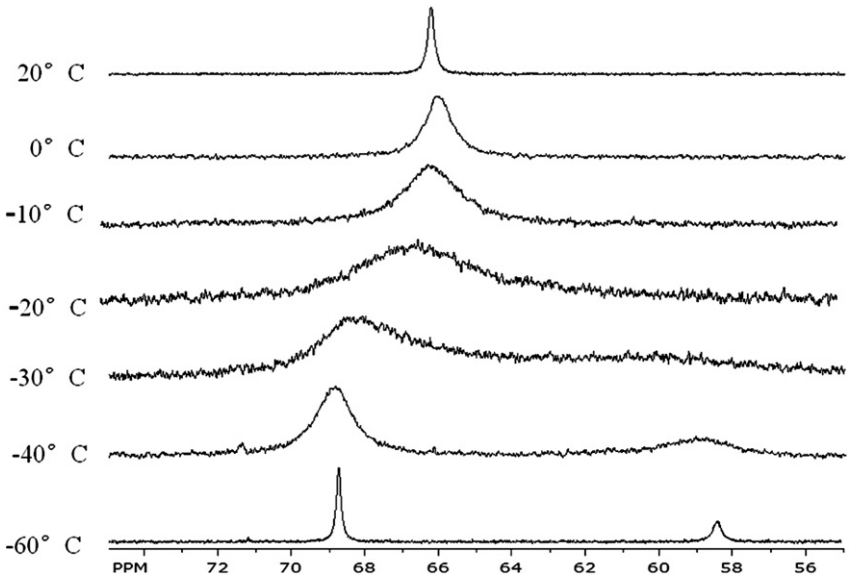

Fig. 4. ^{31}P {H} NMR spectra for compound **3** in CD_2Cl_2 solvent at various temperatures.

tetrahedron with three one electron $Au(PPh_3)$ donors, then the cluster contains a total of 60 electrons and the Ir and each of the Ru atoms will formally have 18 electron configurations. Two related $M_4(AuPPh_3)_3$ complexes have been reported. These are $H_2Ru_4(CO)_{12}(AuPPh_3)_3$, **5** [22,23] and $CoRu_3(CO)_{12}(AuPPh_3)_3$, **6** [18]. The structures of the clusters of these two compounds both contain $(AuPPh_3)_3$ groups in which the central Au atom forms a μ_3-bridge across a triangle of the M_4 cluster, **A**, but in **3** the central Au atom bridges the Ir—Ru edge of the transition metal M_4 cluster, **B**.

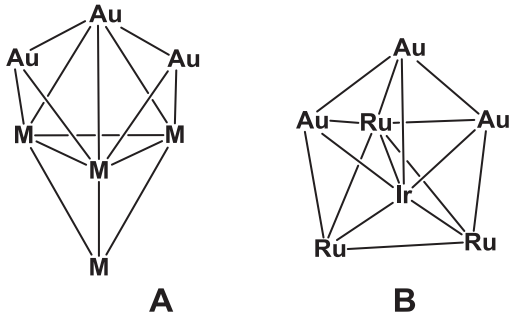

The stoichiometry of the reaction of $[(AuPPh_3)_3O][BF_4]$ with $[PPN][IrRu_3(CO)_{13}]$ is an unusual, in that the monoanion $[IrRu_3(CO)_{13}]^-$ cannot add three $[Au(PPh_3)]^+$ groups and remain uncharged. It is believed that the oxonium oxygen atom of the cation $[(AuPPh_3)_3O]^+$ combines with CO to oxidize it to CO_2. As a result, two electrons are formally released from the oxonium oxygen atom for use in cluster bonding. Thus, the overall reaction that leads to the formation of **3** can be written as shown in eq. (1).

$$[IrRu_3(CO)_{13}]^- + [(AuPPh_3)_3O]^+ \rightarrow IrRu_3(CO)_{12}(AuPPh_3)_3 + CO_2 \quad (1)$$

A similar transformation was proposed for the formation of compound 6 from the reaction of $[(AuPPh_3)_3O][BF_4]$ with $[PPN][CoRu_3(CO)_{13}]$ [18].

As with **2**, the ^{31}P NMR spectrum of **3** exhibits only one phosphorus resonance at room temperature at $\delta = 65.59$, but shows two resonances in a 2/1 ratio resonances as expected at $\delta = 68.47$ (2P) and 58.00 (1P) at −80 °C. As the temperature is raised, the two resonances broaden and coalesce in a process indicative of a dynamical averaging. These spectra are shown in Fig. 4. The broadened spectra were simulated in order to obtain exchange rates and activation parameters for the exchange process. The simulated spectra are shown in Figure S1 in the Supporting Information. From these data the activation parameters were determined $\Delta H^{\ddagger} = 48.8(5)$ kJ·mol^{-1}, $\Delta S^{\ddagger} = 17.3(5)$ J·mol^{-1}K^{-1}. Dynamical activity in polynuclear metal complexes containing $Au(PPh_3)$ groups has been observed previously [22,24,26]. Note: the addition of free PPh_3 to our NMR samples of **3** did not affect the exchange broadened spectra, so a mechanism that involves simple

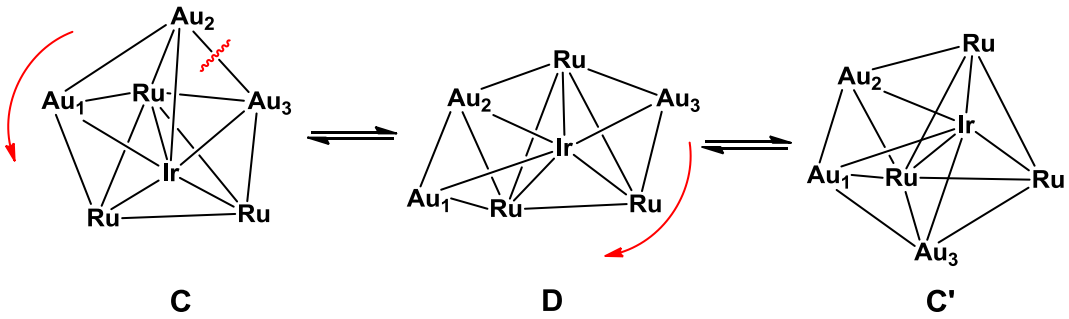

Scheme 3. A proposed mechanism for the dynamical averaging of the $Au(PPh_3)$ groups in compound **3**.

dissociation of PPh_3 from the gold atoms is ruled out. Therefore, a dynamical exchange process that leads to an interchange of the two types $Au(PPh_3)$ groups on the NMR timescale at room temperature seems to be the most likely. A variety of mechanisms can be envisioned, but all must involve the cleavage of at least one of the Au–Au bonds. One mechanism that we find attractive is shown in Scheme 3. Assuming the Au2–Au3 bond is cleaved as in structure **C** on the left and the two bonded Au atoms Au1 and Au2, then pivot around the Ir atom to the position shown in intermediate **D**, the exchange can then be accomplished by shifting atom Au3 to the neighboring $IrRu_2$ triangle with the formation of an Au–Au bond between Au1 and Au3 in the equivalent structure **C′**. In the process Au1 becomes the central Au atom of the Au_3 group and Au2 becomes one of the outer Au atoms. Alternatively, a cleavage of the Au1–Au2 bond in **C** followed by formation of a similar **D** type intermediate (a mirror image of the one shown in Scheme 3) would ultimately lead to the placement of atom Au3 into the center of the Au_3 grouping.

Somewhat similar rocking shifts of $Au_2(PPh_3)_2$ groups have been proposed to explain the averaging of two of the phosphorus resonances in the compound $Ru_6(CO)_{16}(AuPPh_3)_3(\mu_6\text{-}B)$ [25]. It has recently been shown that $Pd(P\text{-}t\text{-}Bu_3)$ groups can migrate from face to face in some polynuclear ruthenium carbonyl cluster complexes [26].

4. Conclusions

The family of mixed transition metal–gold polynuclear metal complexes has been expanded to include the series $H_mIrRu_3Au(PPh_3)_n$, $m = 0/1$, $n = 1–3$. When two or more $Au(PPh_3)$ groups are present in the complex, the $Au(PPh_3)$ groups are mutually bonded to each other and undergo dynamical averaging on the NMR timescale at ambient temperatures. These complexes may serve as precursors to new gold-containing multi-metallic catalysts in the future [27].

Acknowledgments

This research was supported by the National Science Foundation CHE-1111496.

Appendix A. Supplementary material

853373(**2**), 853374(**3**), 853375(**1**) contain the supplementary crystallographic data for this paper. These data can be obtained free of charge from The Cambridge Crystallographic Data Centre via www.ccdc.cam.ac.uk/data_request/cif.

Appendix. Supplementary material

Supplementary data related to this article can be found online at doi:10.1016/j.jorganchem.2012.01.012.

References

[1] (a) R.H. Crabtree, Top. Organomet. Chem. 34 (2011) 1–10;
(b) J.H. Jones, Platinum Metals Rev. 44 (2000) 94–105.
[2] (a) C.M. Jensen, Chem. Commun. (1999) 2443–2449;
(b) V. César, S. Bellemin-Laponnaz, L.H. Gade, Chem. Soc. Rev. 33 (2004) 619–636;
(c) S.-M. Lu, X.-W. Han, Y.-G. Zhou, Adv. Synth. Catal. 346 (2004) 909–912;
(d) W. Matthias, M.W. Haenel, S. Oevers, K. Angermund, W.C. Kaska, H.-J. Fan, M.B. Hall, Angew. Chem. Int. Ed. 40 (2001) 3596–3600.
[3] (a) J. Lu, P. Pedro Serna, C. Aydin, N.D. Browning, B.C. Gates, J. Am. Chem. Soc. 133 (2011) 16186–16195;
(b) B.C. Gates, Chem. Rev. 95 (1995) 511–522;
(c) E. Bayram, M. Zahmakiran, S. Ozkar, R.G. Finke, Langmuir 26 (2011) 12455–12464;
(d) A. Uzun, D.A. Dison, B.C. Gates, ChemCatChem. 3 (2011) 95–107;
(e) B.C. Gates, in: R.D. Adams, F.A. Cotton (Eds.), Catalysis by Di- and Polynuclear Metal Complexes, Wiley-VCH Publishers, New York, 1998 Ch. 14.
[4] R. Psaro, C. Dossi, R. Della Pergola, L. Garlaschelli, S. Calmotti, S. Marngo, M. Bellatreccia, R. Zanoni, Appl. Catal. A: Gen. 121 (1995) L19–L23.
[5] G. Süss-Fink, S. Haak, V. Ferrand, H. Stoeckli-Evans, J. Molec. Catal. 143 (1999) 163–170.
[6] H. Hamada, Y. Kuwahara, Y. Kintaichi, T. Ito, K. Wakabayashi, H. Iljima, K.-I. Sano, Chem. Lett. (1984) 1611–1612.
[7] R.E. Fuentes, J. Farell, J.W. Weidner, Electrochem. Solid-State Lett. 14 (2011) E5–E7.
[8] (a) M. Haruta, Catal. Today 36 (1997) 153–166;
(b) M. Haruta, M. Date, Appl. Catal. A: Gen. 222 (2001) 427–437;
(c) A.S.K. Hashmi, G.J. Hutchings, Angew. Chem. Int. Ed. 45 (2006) 7896–7936.
[9] (a) G.J. Hutchings, Angew. Chem. Int. Ed. (2008) 1148–1164;
(b) L.B. Ortiz-Soto, O.S. Alexeev, M.D. Amiridis, Langmuir 22 (2006) 3112–3117.
[10] (a) T. Chihara, M. Sato, H. Konomoto, S. Kamiguchi, H. Ogawa, Y. Wakatsuki, J. Chem. Soc. Dalton Trans. (2000) 2295–2299;
(b) J.R. Galsworthy, A.D. Hattersley, C.E. Housecroft, A.L. Rheingold, A. Waller, J. Chem. Soc. Dalton Trans. (1995) 549–557.
[11] R.D. Adams, Q. Zhang, Z. Yang, J. Am. Chem. Soc. 133 (2011) 15950–15953.
[12] G. Süss-Fink, S. Haak, V. Ferrand, H. Stoeckli-Evans, J. Chem. Soc. Dalton Trans. (1997) 3861–3865.
[13] L. Malatesta, L. Naldini, G. Simonetta, F. Cariati, Coord. Chem. Rev. 1 (1966) 255–262.
[14] A.N. Nesmeyanov, E.G. Perevalova, Y.T. Struchkov, M.Y. Antipin, K.I. Grandberg, V.P. Dyadchenko, J. Organomet. Chem. 201 (1980) 343–349.
[15] (a) Kirk Marat, SpinWorks 3.1.7 Copyright ©, University of Manitoba, 2010;
(b) A.R. Quirt, J.S. Martin, J. Magn. Reson. 5 (1971) 318–327.
[16] SAINT+, Version 6.2a, Bruker Analytical X-ray Systems, Inc., Madison, WI, 2001.
[17] G.M. Sheldrick, SHELXTL, Version 6.1, Bruker Analytical X-ray Systems, Inc., Madison, WI, 1997.
[18] M.I. Bruce, B.K. Nicholson, Organometallics 3 (1984) 101–108.
[19] (a) R. Bau, M.H. Drabnis, Inorg. Chim. Acta 259 (1997) 27–50;
(b) R.G. Teller, R. Bau, Struct. Bonding 44 (1981) 1–82.
[20] (a) M.J. Freeman, A.G. Orpen, I.D. Salter, J. Chem. Soc. Dalton Trans. (1987) 379–390;
b) A.G. Orpen, I.D. Salter, Organometallics 10 (1991) 111–117.
[21] P. Bellon, M. Manassero, M. Sansoni, J. Chem. Soc. Dalton Trans. (1973) 2423–2427.
[22] J.A.K. Howard, I.D. Salter, F.G.A. Stone, Polyhedron 3 (1984) 567–573.
[23] M.I. Bruce, B.K. Nicholson, J. Organomet. Chem. 252 (1983) 243–255.
[24] (a) I.D. Salter, in: E.W. Abel, F.G.A. Stone, G. Wilkinson (Eds.), Comprehensive Organometallic Chemistry, Vol. 10, Elsevier, London, 1995 Ch. 5;
(b) I.D. Salter, in: P. Braunstein, L.A. Oro, P.R. Raithby (Eds.), Metal Clusters in Chemistry, Vol. 1, Wiley-VCH, Weinheim, 1999, pp. 509–534 Ch. 1.27.
[25] C.E. Housecroft, D.M. Matthews, A. Waller, A.J. Edwards, A.L. Rheingold, J. Chem. Soc. Dalton Trans. (1993) 3059–3070.
[26] R.D. Adams, B. Captain, W. Fu, P.J. Pellechia, M.D. Smith, Inorg. Chem. 42 (2003) 2094–2101.
[27] J. Evans, J. Gao, J. Chem. Soc. Chem. Commun. (1985) 39–40;
(b) Y. Li, W.-X. Pan, W.-T. Wong, J. Cluster Sci. 13 (2002) 223–233.